Microstructures and microwave dielectric properties of Mg_2SiO_4–$Ca_{0.9}Sr_{0.1}TiO_3$ ceramics

Ling Liu · Yongbao Feng · Tai Qiu ·
Xiaoyun Li

Abstract The microstructures and microwave dielectric properties of $(1 - x)Mg_2SiO_4$–$xCa_{0.9}Sr_{0.1}TiO_3$ ($x = 0.05$–0.08) composite ceramics, prepared via a conventional solid-state ceramic route, were investigated. As expected, an increase in sintering temperature effectively promoted densification and enhanced the dielectric properties of the $(1 - x)$ Mg_2SiO_4–$xCa_{0.9}Sr_{0.1}TiO_3$ ceramics used in this study. As the amount of $Ca_{0.9}Sr_{0.1}TiO_3$ increased, temperature coefficient of resonant frequency (τ_f) increased; with a near-zero τ_f obtained for samples where $x = 0.06$. The optimal microwave dielectric properties, a dielectric constant (ε_r) of 8.01, high quality factor ($Q \times f$) of 58,389 GHz (at 14.6 GHz) and a τ_f of -3.62 ppm/°C, were obtained for $0.94Mg_2SiO_4$–$0.06Ca_{0.9}Sr_{0.1}TiO_3$ sintered at 1,440 °C for 3 h.

1 Introduction

Recently, much attention has been drawn to the development of millimeter-wave telecommunications, which have

L. Liu · Y. Feng (✉) · T. Qiu · X. Li
College of Materials Science and Engineering, Nanjing Tech University, No. 5 Xinmofan Road, Nanjing 210009, China
e-mail: fengyongbao@163.com

L. Liu
e-mail: LiuLing606060@hotmail.com

T. Qiu
e-mail: qiutai@njtech.edu.cn

X. Li
e-mail: lixiaoyun@njtech.edu.cn

Y. Feng
Economic Development Zone, Nanjing Sanle Electronic Information Industry Group Co., Ltd, No. 5 Guangming Road, Pukou, Nanjing 211800, China

the potential to transport a large amount of information with high data transfer rates. In order to satisfy this application, the microwave dielectric materials require a low dielectric constant (ε_r), a high quality factor $Q \times f$ for achieving frequency selectivity and stability, and a near-zero temperature coefficient of resonant frequency (τ_f) for temperature stability [1–8].

Silicates with low ε_r are good candidate dielectrics for millimeter-wave applications. Forsterite (Mg_2SiO_4) is a silicate ceramic and has attracted a great deal of attention as a result of its low ε_r (≈ 6.8) and high $Q \times f$ (240,000 GHz). However, Forsterite has a large negative τ_f value (~ -70 ppm/°C) [9], which limits its applicability. Some investigations have been made to adjust the τ_f value of Forsterite to closer to 0 ppm/°C by combining it with TiO_2 [10], $CaTiO_3$ [11], or $Ba_3(VO_4)_2$ [12], which have positive temperature coefficients of resonance frequency. In the present work, $0.91Mg_2SiO_4$–$0.09CaTiO_3$ composite ceramics with Bi_2O_3–Li_2CO_3–H_3BO_3 additions show good microwave dielectric properties ($\varepsilon_r \sim 7.7$, $Q \times f \sim 11,300$ GHz ($f = 6.1$ GHz) and $\tau_f \sim -5.0$ ppm/°C) [11]. A ε_r of 9.03, a $Q \times f$ of 52,500 GHz and a τ_f of 0.6 ppm/°C were obtained for $0.55Mg_2SiO_4$–$0.45Ba_3$ $(VO_4)_2$ ceramics [12]. However, V_2O_5 is used as an important raw chemical in the synthesis of $Ba_3(VO_4)_2$ and it is harmful to our health and to the environment. In this paper, $Ca_{0.9}Sr_{0.1}TiO_3$ ($\varepsilon_r \sim 170$, $Q \times f \sim 8,319$ GHz and $\tau_f \sim 931$ ppm/°C) [13], exhibiting a higher $Q \times f$ than $CaTiO_3$, was added to the Mg_2SiO_4 as a τ_f compensator. As reported, by adjusting the stoichiometry (Mg/Si = 2.05) in Mg_2SiO_4 ceramics, the formation of a $MgSiO_3$ secondary phase could be suppressed effectively [14]. Therefore, the pure Mg_2SiO_4 was prepared by adjusting stoichiometry (Mg/Si = 2.05). The $(1 - x)Mg_2SiO_4$(Mg/Si = 2.05)–$xCa_{0.9}Sr_{0.1}TiO_3$ system is likely to yield an environmentally-

friendly material with excellent dielectric properties. In this work, microstructure and microwave dielectric properties of $(1-x)Mg_2SiO_4(Mg/Si = 2.05)–xCa_{0.9}Sr_{0.1}TiO_3$ $(x = 0.05–0.08)$ ceramics were investigated.

2 Experimental procedures

$(1-x)Mg_2SiO_4(Mg/Si = 2.05)–xCa_{0.9}Sr_{0.1}TiO_3$ $(x = 0.05, 0.06, 0.07$ and $0.08)$ composite ceramics were prepared using a conventional solid-state reaction method. Both Mg_2SiO_4 $(Mg/Si = 2.05)$ and $Ca_{0.9}Sr_{0.1}TiO_3$ compounds were individually synthesized using reagent-grade powders: MgO (98.0 %), SiO_2 (99.5 %), $CaCO_3$ (99.0 %) and TiO_2 (99.0 %). $Mg_2SiO_4(Mg/Si = 2.05)$ and $Ca_{0.9}Sr_{0.1}TiO_3$ were weighed according to the above formula and then ball milled for 6 h whilst submersed in distilled water using zirconia balls, calcined for 4 h at 1,240 and 1,100 °C respectively. After this, the $(1-x)Mg_2SiO_4$ $(Mg/Si = 2.05)–xCa_{0.9}Sr_{0.1}TiO_3$ mixtures were prepared by mixing $Ca_{0.9}Sr_{0.1}TiO_3$ and Mg_2SiO_4 powders with several weight ratios. The mixtures were then ball milled for 6 h using zirconia balls in distilled water. After drying, the fine powders were mixed with appropriate PVA binders and pressed into pellets (11 mm in diameter and 5 mm in thickness) at 300 MPa. The pellets were then sintered at 1,380–1,500 °C for 3 h in air.

The crystalline phase compositions of the sintered samples were investigated by X-ray diffraction (XRD), using Cu Kα radiation [RIGAKU SmartLab(3)]. The surface microstructure of the thermally etched specimens was observed using a JEOL (JSM-5900) scanning electron microscopy (SEM) equipped with a NORAN VANTAGE DSI energy dispersive spectroscope (EDS). The bulk density of the sintered samples was measured using the Archimedean method. The dielectric properties of the samples at microwave frequency were measured using a network analyzer (AGILENT 8722ET) and analyzed using the modified Hakki and Coleman and Courtney's methods [15, 16]. τ_f was evaluated in the temperature range of 25–80 °C. It was determined by noting the change in resonant frequency and using the following equation:

$$\tau_f = \frac{f_{80} - f_{25}}{f_{25} \times 55} \times 10^6 (ppm/°C)$$

where f_{25} and f_{80} represent resonant frequencies at temperatures 25 and 80 °C, respectively.

3 Results and discussion

Figure 1 illustrates the apparent porosity and bulk densities of the $(1-x)Mg_2SiO_4–xCa_{0.9}Sr_{0.1}TiO_3$ ceramics sintered at 1,380–1,500 °C. The bulk densities increase as the x
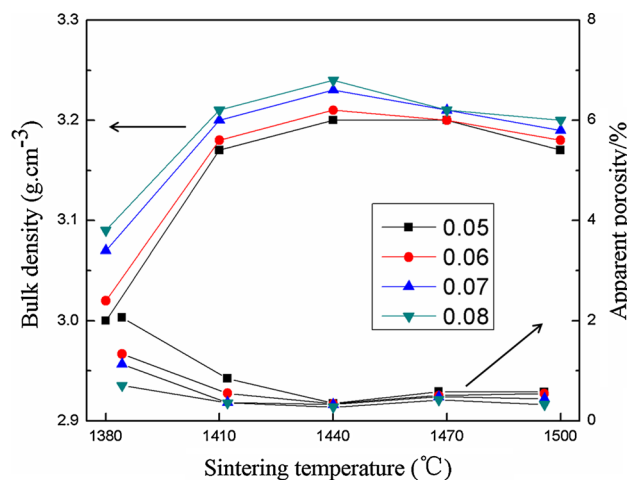
Fig. 1 Apparent porosity and bulk density of $(1-x)Mg_2SiO_4–xCa_{0.9}Sr_{0.1}TiO_3$ ceramics as a function of sintering temperature
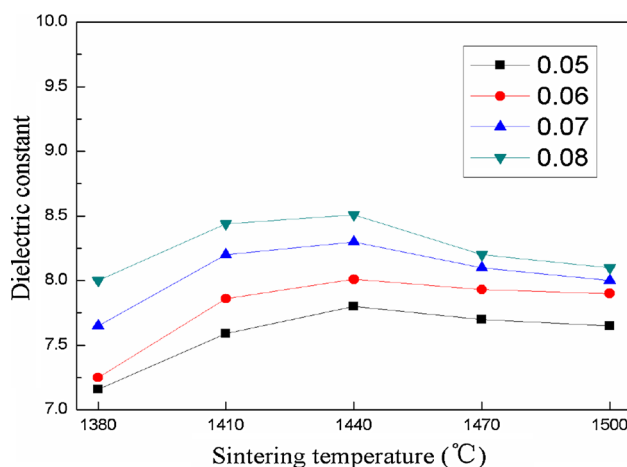
Fig. 2 Dielectric constant of $(1-x)Mg_2SiO_4–xCa_{0.9}Sr_{0.1}TiO_3$ ceramics as a function of sintering temperature

values increase from 0.05 to 0.08, largely due to an increase in the $Ca_{0.9}Sr_{0.1}TiO_3$ content. The theoretical density of a Mg_2SiO_4 ceramic is 3.223 g/cm³, whereas the density of $Ca_{0.8}Sr_{0.2}TiO_3$ is higher at 4.082 g/cm³. This suggests that the higher $Ca_{0.9}Sr_{0.1}TiO_3$ content would show a relatively higher density in the ceramics. It also can be observed that the apparent porosity decreases and then increases minimally with an increase in sintering temperature, In contrast, the densities increase and then decrease with an increase in sintering temperature. The minimum apparent porosity and subsequent maximum densities of samples are obtained at 1,440 °C; likely to be due to the well-developed grain growth, as illustrated in Fig. 7.

Figures 2 and 3 show that ε_r and $Q \times f$ of $(1-x)Mg_2SiO_4–xCa_{0.9}Sr_{0.1}TiO_3$ ceramics separately. The trend seen in the increase in dielectric constant with an increase in the proportion of the $Ca_{0.9}Sr_{0.1}TiO_3$ phase is in agreement with
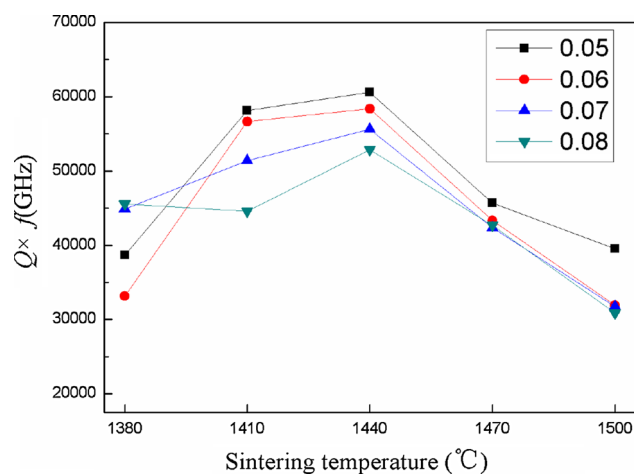
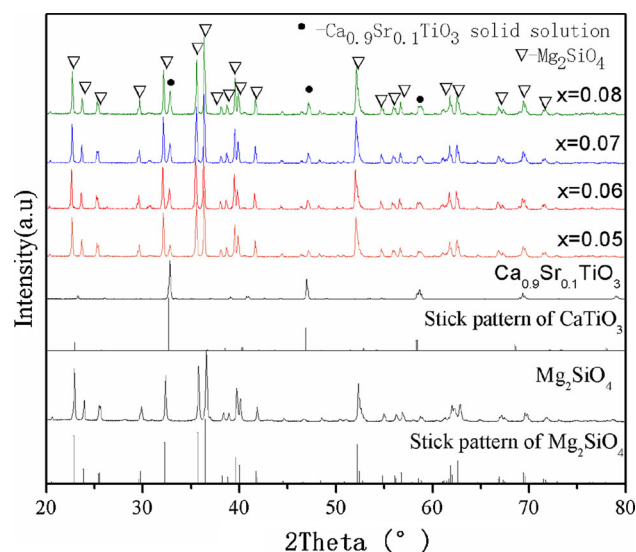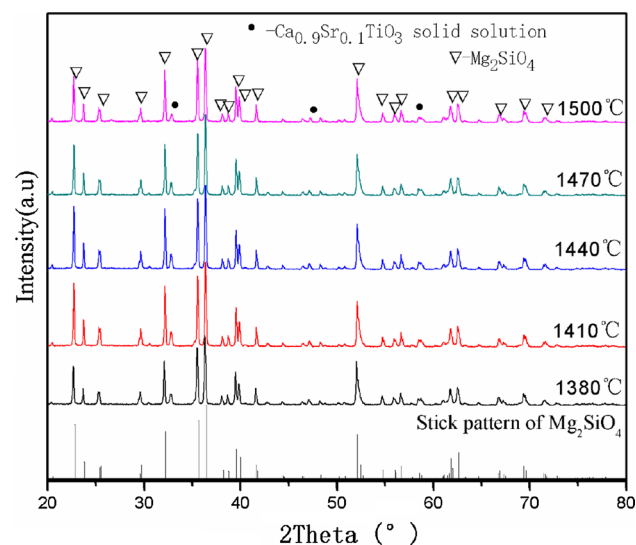**Fig. 3** $Q \times f$ of $(1 - x)Mg_2SiO_4-xCa_{0.9}Sr_{0.1}TiO_3$ ceramics as a function of sintering temperature
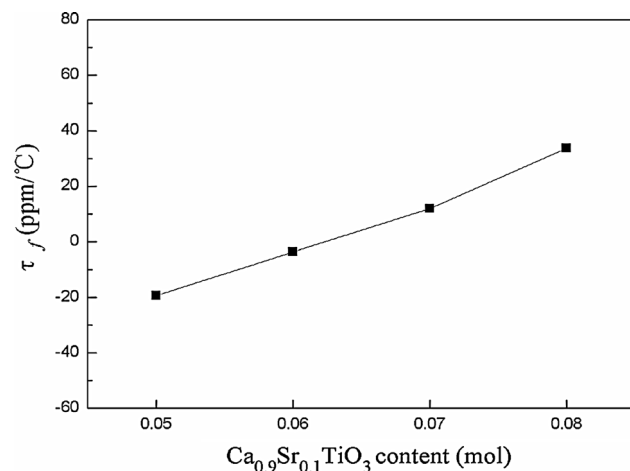
Fig. 4 τ_f of $(1 - x)Mg_2SiO_4-xCa_{0.9}Sr_{0.1}TiO_3$ ceramics as a function of sintering temperature

Fig. 5 XRD patterns of $(1 - x)Mg_2SiO_4-xCa_{0.9}Sr_{0.1}TiO_3$ ceramics with different x values, Mg_2SiO_4 powder and $Ca_{0.9}Sr_{0.1}TiO_3$ powder sintered at 1,440 °C for 3 h
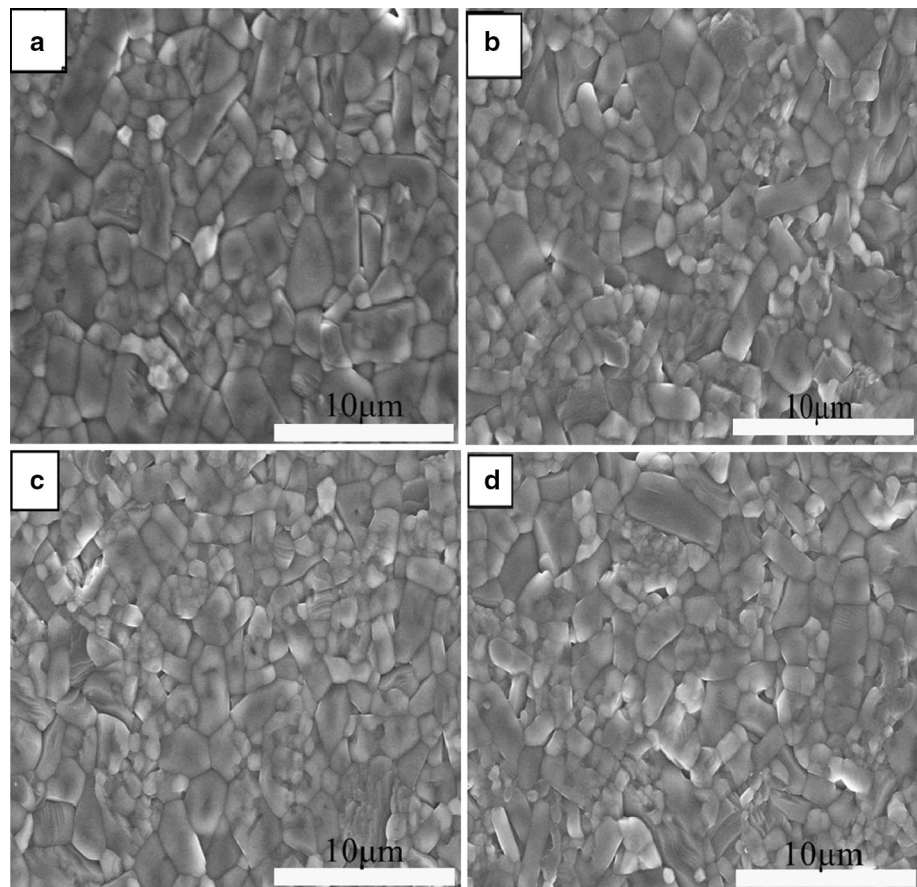

Fig. 6 XRD patterns of $0.94Mg_2SiO_4-0.06Ca_{0.9}Sr_{0.1}TiO_3$ ceramics sintered at different temperatures for 3 h

predictions, owing to the higher ε_r value of $Ca_{0.9}Sr_{0.1}TiO_3$. Where sintering temperatures were increased from 1,380 to 1,500 °C, ε_r values increased to a maximum and subsequently decreased. The maximum ε_r values for the $(1 - x)Mg_2SiO_4-xCa_{0.9}Sr_{0.1}TiO_3$ ceramics were obtained at 1,440 °C. This is likely to be a result of the densification of the ceramics having a greater influence on their ε_r as ε_r increases when the bulk densities of samples increase.

$Q \times f$ values showed a similar trend with a variation in bulk density of the samples as a function of sintering temperature (Fig. 3). $Q \times f$ values increase to a maximum then subsequently decrease. At lower temperatures, the reduction of $Q \times f$ is due to a change in porosity and overall bulk density. However, at higher temperatures, the reduction of $Q \times f$ is largely due to porosity as well as abnormal grain growth, which can be seen in Figs. 1 and 8e.

Figure 4 illustrates the variation in τ_f for $(1 - x)Mg_2SiO_4-xCa_{0.9}Sr_{0.1}TiO_3$ ceramics sintered at 1,440 °C as a function of x value. τ_f increases from -19.29 to 33.7 ppm/°C with an increase in the $Ca_{0.9}Sr_{0.1}TiO_3$ content. Moreover, this trend in the variation of τ_f is consistent with the Lichtenecker empirical rule. As reported, τ_f for Mg_2SiO_4 is -70 ppm/°C and τ_f for $Ca_{0.9}Sr_{0.1}TiO_3$ is 931 ppm/°C. In addition, a near-zero τ_f (-3.62 ppm/°C) is obtained for $0.94Mg_2SiO_4-0.06Ca_{0.9}Sr_{0.1}TiO_3$ ceramics sintered at 1,440 °C for 3 h.

Figure 5 shows XRD patterns for $(1 - x)Mg_2SiO_4-xCa_{0.9}Sr_{0.1}TiO_3$ composite ceramics, Mg_2SiO_4 powder and $Ca_{0.9}Sr_{0.1}TiO_3$ powder sintered at 1,440 °C for 3 h. Figure 6

Fig. 7 SEM photographs of $(1 - x)Mg_2SiO_4$–$xCa_{0.9}Sr_{0.1}TiO_3$ ceramics with different sintered at 1,440 °C for 3 h in air: **a** $x = 0.05$, **b** $x = 0.06$, **c** $x = 0.07$, **d** $x = 0.08$

Table 1 The EDS data of the spots A, B marked in Fig. 8c

| Spots	Atom (%)					
	O–K	Mg–K	Si–K	Ca–K	Ti–K	Sr–L
A	58.90	27.59	13.51			
B	58.52	16.15	8.05	7.63	8.8	0.85

shows XRD patterns for $0.94Mg_2SiO_4$–$0.06Ca_{0.9}Sr_{0.1}TiO_3$ ceramics sintered at different temperatures for just 3 h. All the main peaks can be indexed using the perovskite structure (orthorhombic: ICDD-PDF no. 82-0231) and Mg_2SiO_4 (orthorhombic: ICDD-PDF no. 04-0768). XRD phase analysis reveals that $Ca_{0.9}Sr_{0.1}TiO_3$ and Mg_2SiO_4 coexist in a sintered composite ceramic and no other crystalline phases are detected. XRD phase analysis also shows that the $MgSiO_3$ secondary phase could be suppressed by adjusting the ratio of Mg/Si in the Mg_2SiO_4 ceramics [14]. The intensities of the diffraction peaks of the $Ca_{0.9}Sr_{0.1}TiO_3$ phases do not vary dramatically with an increase in the proportion of $Ca_{0.9}Sr_{0.1}TiO_3$ in the compound. This is likely to be because the content of $Ca_{0.9}Sr_{0.1}TiO_3$ is only small and varies only within a small range. Perovskite and Mg_2SiO_4 phases are observed for all samples, indicating that the

sintering temperature has little influence on the composition of the $0.94Mg_2SiO_4$–$0.06Ca_{0.9}Sr_{0.1}TiO_3$ ceramics.

Figure 7a–d illustrates the representative SEM micrographs of $(1 - x)Mg_2SiO_4$–$xCa_{0.9}Sr_{0.1}TiO_3$ ($x = 0.05$, 0.06, 0.07 and 0.08) composite ceramics sintered at 1,440 °C for 3 h. All micrographs exhibit ceramics with dense microstructures with only small pores in Fig. 7a. However, the grain size is not uniformly distributed in all of the samples. The SEM micrographs of the $0.94Mg_2SiO_4$–$0.06Ca_{0.9}Sr_{0.1}TiO_3$ ceramics, sintered at different temperatures for 3 h, are shown in Fig. 8a–e. The number of pores decrease with an increase in sintering temperature from 1,380 to 1,470 °C. However, when the sintering temperature increases to 1,500 °C, the number of pores increases oppositely. In addition, the grain size increases abnormally (Fig. 8e), resulting in a decrease in $Q \times f$. The samples with well-developed grain growth and dense microstructures are obtained at 1,440 °C for 3 h. In order to further verify the proportion of $(1 - x)Mg_2SiO_4$–$xCa_{0.9}Sr_{0.1}TiO_3$ composite ceramics, the grains were analyzed using EDS. The EDS data is shown in Table 1 and is marked in Fig. 8c. Based on the EDS analyses, the grain marked A is Mg_2SiO_4 and that marked B is Mg_2SiO_4 and $Ca_{0.9}Sr_{0.1}TiO_3$, which could be certified by the ratios of

Fig. 8 SEM photographs of $0.94Mg_2SiO_4$– $0.06Ca_{0.9}Sr_{0.1}TiO_3$ ceramics sintered at different temperatures for 3 h in air: **a** 1,380 °C, **b** 1,410 °C, **c** 1,440 °C, **d** 1,470 °C, **e** 1,500 °C
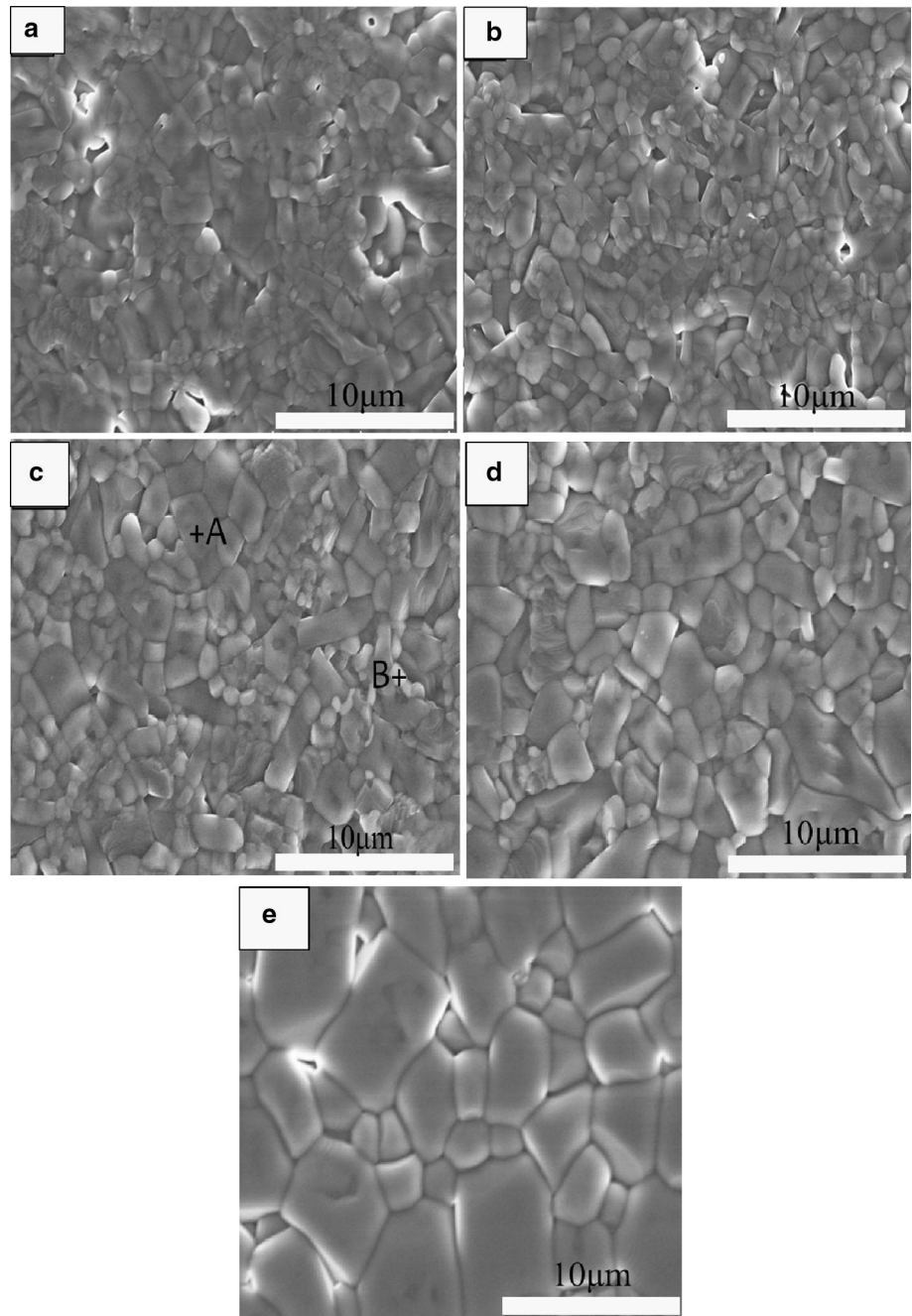
Mg:Si:O and Ca:Sr:Ti:O that are approximately 2:1:4 and 9:1:10:30 respectively. The observations of SEM and EDS are consistent with the XRD results shown in Fig. 5.

4 Conclusions

In this study, for the purpose of adjusting τ_f values, $Ca_{0.9}Sr_{0.1}TiO_3$ was added to Mg_2SiO_4. The microstructure and microwave dielectric properties of the $(1 - x)Mg_2SiO_4$–$xCa_{0.9}Sr_{0.1}TiO_3$ ($x = 0.05$–0.08) ceramics were

investigated as a function of composition (x) and sintering temperature. All the samples exhibited two crystalline phases: Perovskite and Forsterite. The microwave dielectric prosperities and bulk densities were found to be associated with the varying contents of $Ca_{0.9}Sr_{0.1}TiO_3$ and sintering temperatures. At the composition of $x = 0.06$, the $0.94Mg_2SiO_4$–$0.06Ca_{0.9}Sr_{0.1}TiO_3$ ceramics sintered at 1,440 °C for 3 h show excellent microwave dielectric properties ($\varepsilon_r = 8.01$, $Q \times f = 58,389$ GHz and $\tau_f = -3.62$ ppm/°C), indicating that they could be used as candidate materials for many applications.

References

1. R.J. Cava, J. Mater. Chem. **11**, 54–62 (2001)
2. T. Fujii, A. Ando, Y. Sakabe, J. Eur. Ceram. Soc. **26**, 1857–1860 (2006)
3. T. Fujii, A. Ando, Y. Sakabe, Jpn. J. Appl. Phys. **43**, 6765–6768 (2004)
4. H. Ohsato, T. Tsunooka, A. Kan, Y. Ohishi, Y. Miyauchi, Y. Tohdo, T. Okawa, K. Kakimoto, H. Ogawa, Key Eng. Mater. **269**, 195–198 (2004)
5. K.X. Song, X.M. Chen, C.W. Zheng, Ceram. Int. **34**, 917–920 (2008)
6. M.E. Song, J.S. Kim, M.R. Joung, S. Nahm, J. Am. Ceram. Soc. **91**, 2747–2750 (2008)
7. L. Cheng, P. Liu, X.M. Chen, J. Alloys Compd. **513**, 373–377 (2012)
8. J. Sugihara, K. Kakimoto, I. Kagomiya, H. Ohsato, J. Eur. Ceram. Soc. **27**, 3105–3108 (2007)
9. T. Tsunooka, T. Sugiyama, H. Ohsato, K. Kakimoto, M. Andou, Y. Higashida, H. Sugiura, Key Eng. Mater. **269**, 199–202 (2004)
10. I. Kagomiya, J. Sugihara, K. Kakimoto, H. Ohsato, J. Electroceramics **22**, 327–333 (2009)
11. G. Dou, D. Zhou, M. Guo, S. Gong, Y. Hu, J. Mater. Sci. Mater. Electron. **24**, 1431–1438 (2013)
12. S.Q. Meng, Z.X. Yue, H. Zhuang, F. Zhao, L.T. Li, J. Am. Ceram. Soc. **93**, 359–361 (2010)
13. P.L. Wise, I.M. Reaney, W.E. Lee, T.J. Price, D.M. Iddles, D.S. Cannell, J. Eur. Ceram. Soc. **21**, 1723–1726 (2001)
14. K.X. Song, X.M. Chen, X.C. Fan, J. Am. Ceram. Soc. **90**, 1808–1811 (2007)
15. B.W. Hakki, P.D. Coleman, IEEE Trans. Microw. Theory Tech. **8**, 402–410 (1960)
16. W.E. Courtney, IEEE Trans. Microw. Theory Tech. **18**, 476–485 (1970)